analytical chemistry

Article

Cite This: *Anal. Chem.* 2019, 91, 8540−8548

pubs.acs.org/ac

A Divide-and-Conquer Strategy for Quantification of Light Absorption, Scattering, and Emission Properties of Fluorescent Nanomaterials in Solutions

Joanna Xiuzhu Xu,[†] Yucheng Yuan,[Δ] Shengli Zou,[§] Ou Chen,[Δ] and Dongmao Zhang*[,†,⊥]

[†]Department of Chemistry, Mississippi State University, Mississippi State, Mississippi 39762, United States

[Δ]Department of Chemistry, Brown University, 324 Brook Street, Providence, Rhode Island 02912, United States

[§]Department of Chemistry, University of Central Florida, Orlando, Florida 32816, United States

[⊥]Department of Chemistry, Xihua University, Chengdu, 610039, China

Supporting Information

ABSTRACT: Optical properties of fluorescent materials including their UV−vis absorption, scattering, and on-resonance fluorescence activities are strongly wavelength-dependent. Reported herein is a divide-and-conquer strategy for experimental quantification of fundamental optical constants of fluorescent nanomaterials including their UV−vis absorption, scattering, and on-resonance-fluorescence (ORF) cross-section spectra and ORF fluorescence and light scattering depolarization spectra. The fluorophore UV−vis extinction spectrum is first divided into a blue and a red wavelength region. The UV−vis extinction cross-section spectrum in the blue wavelength region is decomposed into its absorption and scattering extinction spectra straightforwardly using the established polarized resonance synchronous spectroscopic technique. In its red wavelength region, however, the fluorophores can be simultaneous photon absorbers, scatterers, and anti-Stokes-shifted, on-resonance, and Stokes-shifted fluorescence emitters under the resonance excitation and detection conditions. A polarized anti-Stokes'-shifted, on-resonance, and Stokes'-shifted spectroscopic method is developed for quantifying fluorophore absorption, scattering, one-resonance fluorescence (ORF) cross-section spectra, and scattering and ORF fluorescence depolarization spectra in this wavelength region. Example applications of the presented techniques were demonstrated with fluorescent polystyrene nanoparticles, fluorescent quantum dots, and molecular fluorophores Rhodamine 6G and Eosin Y.

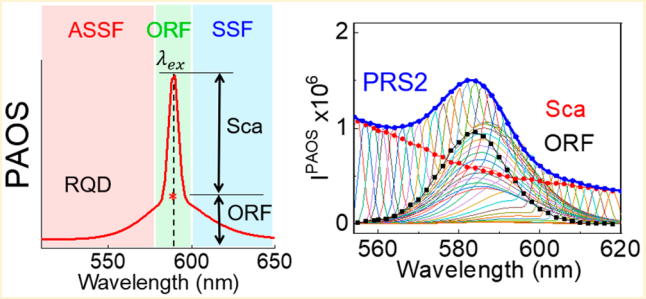

Nanoscale fluorescent materials have become increasingly interesting for their applications in optical sensing, imaging, optoelectronics, energy harvesting, and photocatalytic reactions.[1−8] Understanding the optical properties of fluorescent nanomaterials is important for rational material design and applications. However, reliable quantifications of fluorophore photon absorption, scattering, and fluorescence activities can be challenging due to the complex interplay of the photon absorption, scattering, and emission. As an example, the UV−vis spectrophotometric measurements quantify the sample total photon extinction, the combined contributions by material photon absorption and scattering. It is, however, a widespread practice for researchers to explicitly label or interpret the experimental UV−vis extinction spectra as absorbance spectra. This approach can be highly problematic for nanoscale materials whose light scattering is likely significant.[9−14] In cases where light scattering was considered, some researchers assume that fluorescent nanoparticles (NPs) are Rayleigh scatterers in the long wavelength region and then compute the fluorophore scattering activities in the short wavelength by assuming its scattering cross-section linearly proportional to λ^{-4}.[15] The validity of this approach has not been examined, to our knowledge. Indeed, light scattering is a universal material property because all materials have nonzero polarizability.[16,17] Furthermore, only nonabsorbing materials with sizes significantly smaller than excitation wavelengths can be approximated as Rayleigh scatterers.[18] Resonance light scattering can occur for light-absorbing materials in the wavelength region where the sample absorbs.[17] Such resonance light scattering has been extensively demonstrated in nanoscale fluorophore aggregates such as self-assembled porphyrins.[19−23]

While there are many analytical techniques for detecting sample light scattering intensity, scant information is available on material scattering cross-sections. As an example, light scattering cross-section spectra of common organic solvents have been made available only very recently.[24] Compared to solvents, most of which are approximately pure scatterers with no significant photon absorption and emission in the UV−vis

Received: April 12, 2019
Accepted: May 28, 2019
Published: May 28, 2019

DOI: 10.1021/acs.analchem.9b01803
Anal. Chem. 2019, 91, 8540−8548

region, quantification of optical properties of fluorescent materials is drastically more difficult. A series of challenges must be simultaneously addressed in order to reliably determine their light scattering cross-section spectra. The first is the sample inner filter effect (IFE) induced by the sample photon absorption.[25,26] The second is the interference of light scattering by solvent and sample holders. The third is the under-sampling issue arising from the fact that a spectrofluorometer collects only a small fraction of the scattered and/or emitted photons that are distributed in the three-dimensional space.[27] Critically, the fraction of the collected photons versus the total number of scattered or emitted photons depends not only on the instrument setups (e.g., acceptance angle, detection geometry, detection polarization bias) but also on the sample light scattering and fluorescence depolarization. Indeed, one must quantify the material light scattering and fluorescence depolarization in order to determine its light scattering and fluorescence activities.[27] The fourth is the interference of fluorophore fluorescence on light scattering detection. Such fluorescence interference arises from the fact that, when excited in the wavelength region it both absorbs and emits, a fluorophore can produce both fluorescence emission and light scattering under resonance excitation and detection conditions.[27−29]

A recent advance in the experimental quantification of the material optical properties is the polarized resonance synchronous spectroscopic (PRS2) technique.[27,30] Like the conventional resonance synchronous spectroscopic (RSS) method, PRS2 spectrum is also acquired with spectrofluorometers under resonance excitation and detection conditions. Unlike the RSS method that uses plane polarized light (also commonly referred to as collimated nonpolarized light) for excitation and detection, however, the excitation and detection photons in PRS2 measurements are both linearly polarized.[27] For nonfluorescent materials, the IFE-corrected sample PRS2 signal is due completely to sample light scattering.[27] However, the IFE-corrected PRS2 spectra of fluorescent samples can contain both fluorescence and light scattering.[27] Therefore, one needs to decompose the fluorophore PRS2 spectra into its PRS2 scattering and fluorescence component spectra before quantification of the fluorophore light scattering and fluorescence cross sections and depolarizations.

Understanding the origin of the light scattering signal in PRS2 spectra is straightforward. However, identifying the sources of the fluorescence signal in the sample PRS2 spectrum has proven challenging. As an example, beguiled by the fact the PRS2 is acquired under resonance excitation and detection conditions, we attributed the fluorescence signal in the PRS2 spectrum all to the fluorophore ORF in our initial PRS2 work.[27] Later on, we discovered that the fluorescence signal in the PRS2 spectrum is proportional to the square of the excitation and detection monochromator bandwidth while the light signal in the PRS2 spectrum is linearly proportional to the monochromator bandwidth.[30] This observation leads to the realization that off-resonance fluorescence must also contribute to the fluorescence signal detected under the resonance excitation and detection conditions.[30] Unfortunately, however, we attributed such off-resonance fluorescence completely to fluorophore Stokes-shifted fluorescence (SSF).[30] The possible contribution by the fluorophore anti-Stokes-shifted fluorescence (ASSF) to the fluorescence signal in the PRS2 spectra has not been studied.

Using a new polarized anti-Stokes-shifted, on-resonance, and Stokes-shifted (PAOS) spectroscopic method developed in this work, we provide direct visual evidence that, besides ORF and SSF, fluorophore ASSF also contributes to its PRS2 fluorescence signal. An individual PAOS spectrum is acquired by keeping the excitation wavelength fixed but varying the detection wavelengths from the anti-Stokes' side to the Stokes side of the excitation wavelength. As will be shown later in this work, by acquiring a set of PAOS spectra as a function of excitation wavelength, one can reconstruct the fluorophore PRS2 spectrum and the fluorophore PRS2 light scattering and PRS2 fluorescence component spectra.

While the PAOS spectral acquisition enables visual examination and facile separation of the fluorophore fluorescence and light scattering signal detected under resonance excitation and detection conditions, it can be time-consuming if the PAOS spectral acquisition is implemented crossing the entire UV−vis spectral region. To resolve this issue, we devised a divide-and-conquer approach so that relatively tedious PAOS spectral acquisition is limited to the fluorophore emission wavelength region. This divide-and-conquer strategy divides a fluorophore UV−vis spectrum into a blue and a red wavelength region. The blue wavelength region spans from 300 nm to the blue-edge of the fluorophore SSF peak. The fluorophores in this wavelength region are simultaneous photon absorbers and scatterers, but not emitters under the resonance excitation and detection conditions. The fluorophore red-wavelength region spans from the blue-edge of the fluorophore SSF peak to the red-edge of its SSF peak. In this region, the IFE-corrected PRS2 spectrum can contain fluorophore ASSF, ORF, and SSF emission and light scattering features, as will be demonstrated later.

The five model fluorophores used in this work comprise three NP fluorophores: fluorescence polystyrene NPs (fPSNP), rod-shaped fluorescent quantum dots (RQD), spherical fluorescence quantum dots (SQD), and two molecular fluorophores: Rhodamine 6G (R6G) and Eosin Y (EY). These fluorophores differ significantly in their light scattering, absorption, and ORF activities. Therefore, they serve a representative set of model analytes for testing the utility of the designed methods. For discussion simplicity, all PRS2 and PAOS spectra will be represented as PRS2 XD and PAOS XD, respectively. The first letter X indicates the polarization direction of the excitation linear polarizer, while the second letter D stands for the detection polarizer. Both X and D can take values "N," "V," and "H," where "N" indicates no linear polarizer is used; "V" represents that the light is vertically polarized, i.e, the electrical field of the electromagnetic wave is perpendicular to the spectrofluorometer plane defined by the excitation lamp, sample chamber, and detector; and "H" indicates the linear polarizer is parallel to the instrument plane.

EXPERIMENTAL SECTION

Chemicals and Equipment. R6G and EY were obtained from Sigma-Aldrich and used as received. The polystyrene NPs (PSNPs, Cat#16688) and fPSNPs (Cat# 18719), both with a particle diameter of 0.1 μm, were purchased from Polysciences, Inc. The ligand-stabilized CdSe/CdS core−shell SQDs and RQDs were synthesized in house accroding to published procedure,[31,32] and characterized using the procedures detailed in the Supporting Information.

DOI: 10.1021/acs.analchem.9b01803
Anal. Chem. 2019, 91, 8540−8548

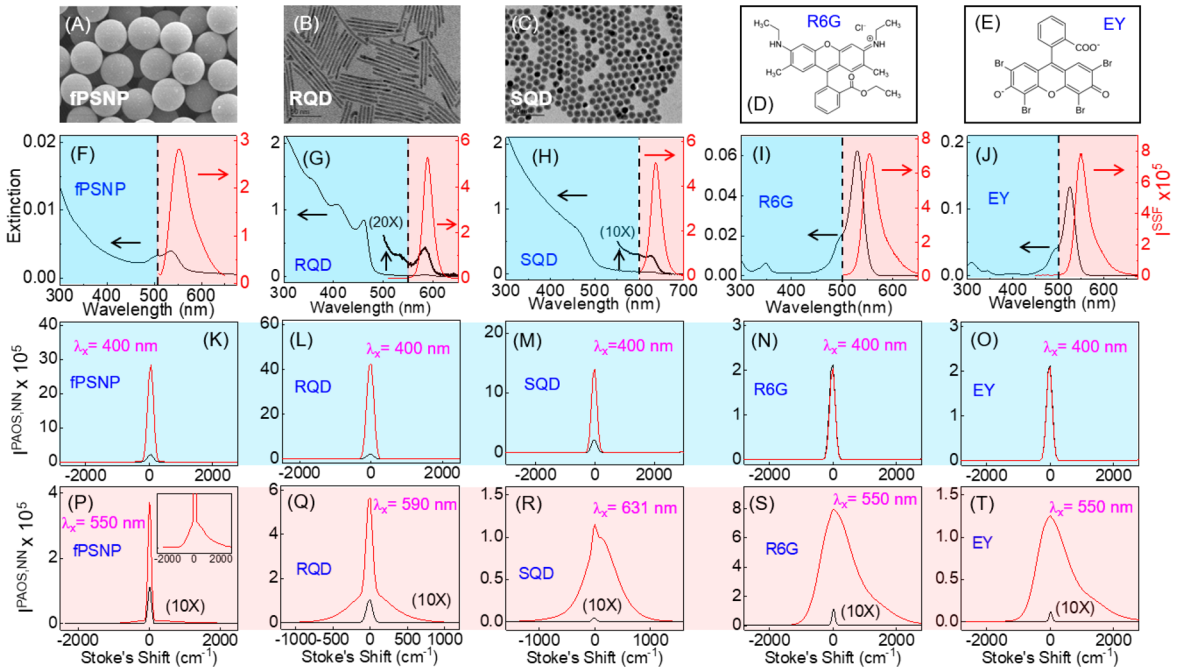

Figure 1. Structures, UV−vis, fluorescence, and PAOS spectra obtained with (1st column) fPSNP, (2nd column) RQD, (3rd column) SQD, (4th column) R6G, and (5th column) EY. (1st row; A, B, and C) TEM images of fPSNP, RQD, and SQD, respectively. (D and E) R6G and EY molecular structures, respectively. (2nd row; black) UV−vis extinction and (red) SSF spectra. The dashed lines divide the blue and red wavelength regions shadowed with blue and pink, respectively. (3rd row and 4th row): Example PAOS spectra obtained with an excitation wavelength in the (3rd row) blue- and (4th row) red-wavelength region. The spectra in red and black are the as-acquired sample and solvent PAOS spectrum, respectively. The solvent PAOS spectra in P−T is scaled by a factor of 10. The inset in P is the zoom-in of the data showing the fPSNP fluorescence signal.

UV−vis, Fluorescence, PRS2, and PAOS Spectral Acquisitions. The UV−vis extinction spectra were obtained with a Thermo Scientific Evoltion 300 UV−vis spectrometer, while the fluorophore fluorescence, PRS2, and PAOS spectra were acquired with a Horiba FluoroMax-4 spectrofluorometer equipped with an excitation and detection linear polarizer. Unless specified otherwise, all the spectrofluorometer-based spectral acquisitions were performed with an intergration time of 0.3 s and a slit width of 2 nm for both the excitation and detection monochromators. The spectral intensity was the ratio of the ratio between the signal from the sample detector and reference detector (S1/R1) .

The PRS2 spectra are acquired with the method described before.[27] Unless specified otherwises, all PAOS and PRS2 spectra data shown in this work are IFE-corrected and solvent- and cuvette-background subtracted using an established method.[27] The effective excitation and detection pathlengths used for the IFE correction were 0.46 and 0.55 cm, respectively,[25,26] which were quantified using a water Raman spectroscopic method.[26] The G-factor spectrum needed to correct the detector polarization bias in the PAOS and PRS2 data analysis was quantified in our previous work.[27]

RESULTS AND DISCUSSION

Fluorophore Optical Properties in Fluorophore Blue Wavelengh Region. Division of the fluorophore UV−vis extinction spectra into their blue and red wavelength regions is straightward on the basis of the fluorophore experimental UV−vis extinction and SSF spectra (Figure 1F−J). The wavelength region below the blue-edge of the SSF peak is the blue wavelength region (highlighted blue in Figure 1F−J). The spectral region covering SSF emission wavelengths is referred to as the red-wavelength region (highlighted red in Figure 1F−J).

In their blue wavelength region, the NP fluorophores fPSNP, RQD, and SQD are simultanously photon absorbers and scatterers but not emitters, while the two molecular fluorophores R6G and EY are predominantly light absorbers with no signficant photon scattering or emissions under the resonance excitation and detection conditions. The light scattering of the NP fluorophores is evident from the intense sharp peak centered at detection wavelength with zero Stokes-shift from excitation wavelength (the blue curve in Figure 1K−M). This peak shares the same shape with the solvent light scattering peak but with drastically higher intensity. In contrast, there is no detectable fluorophore light scattering in the AOS spectra obtained with R6G and EY in their respective blue wavelength regions (Figure 1N−O). The light scattering peaks in these two sample solutions are due almost entirely to light scattering from the solvent and sample-holder background.

In their red wavelength region, NP fluorophores are all simultaneous photon absorbers, scatterers, and fluorescence emitters (Figure 1P−R), while the R6G and EY are simutaneous photon absorbers and emitters with, again, no signficant photon scattering (Figure 1S,T). The absence of detectable photon scattering by R6G and EY is not surprising because of their small sizes. For these two molecular fluorophores, their UV−vis extinction cross-section spectra were directly taken as their respective absorption cross-section spectrum (Figure S2, Supporting Information).

For the NP fluorophores, however, their photon scattering contribution to their UV−vis extinction spectra should be considered in quantification of their photon absorption activities. In other words, one needs to decompose the NP

DOI: 10.1021/acs.analchem.9b01803
Anal. Chem. 2019, 91, 8540−8548

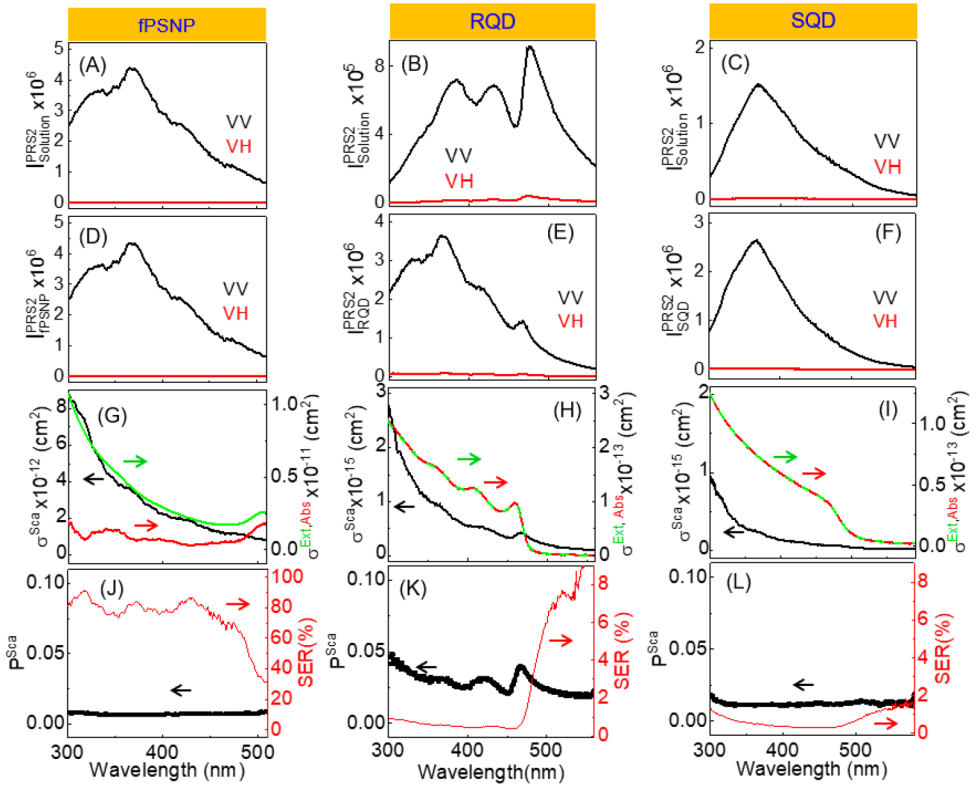

Figure 2. Decomposition of NP fluorophore UV−vis extinction cross-section spectra into the absorption and scattering component spectra for (1st column) fPSNP, (2nd column) RQD, and (3rd column) SQD in their blue wavelength region. (1st row) As-acquired PRS2 (black) VV and (red) VH spectra of the sample solutions. (2nd row) Fluorophore-specific PRS2 (black) VV and (red) VH spectra. (3rd row) UV−vis (green) extinction, (red) absorption, and (black) scattering cross-section spectra. (4th row; red) the fluorophore scattering-to-extinction ratio (SER) and (black) scattering depolarization spectrum.

UV−vis extinction spectra into its absorption and scattering component spectra. The fluorophore PRS2 spectra obtained in their blue wavelength region are due exclusively to the fluorophore light scattering with no fluorescence contribution (Figure 1K−O). As such, one calculates the fluorophore light scattering depolarization spectrum and, subsequently, its scattering cross-section spectra using the experimental PRS2 VV and VH spectra (Figure 2). The procedures for converting the as-acquired solution PRS2 VV and VH spectra (Figure 2A−C) to their respective fluorophore-specific PRS2 spectra (Figure 2D−F), the calculations of the fluorophore light scattering depolarization spectra (Figure 2J−L), and cross-section spectra (Figure 2G−I) are shown in earlier works.[24,33] After quantification of the fluorophore extinction cross-section spectra (Figure 2G−I) on the basis of the fluorophore UV−vis extinction spectra (Figure 1F−H), the fluorophore UV−vis absorption cross-section spectra (Figure 2G−I) were obtained by subtracting the scattering cross-section spectrum from the fluorophore UV−vis extinction cross-section spectrum.

Several obervations are worth noting: First, with only the exception of the fPSNP that is predominatly a photon scatterer in its blue wavelength region, the QD and molecular fluorophores are all strong photon absorbers in their respective blue wavelength regions. The highest scattering-to-extinction ratio is more than 80% for fPSNP (Figure 2G) but 8% (Figure 2H) and 2% (Figure 2I) for RQD and SQD, respectively. These indicate that the examined QDs are predominant photo absorbers. Second, the fPSNPs can be approximated as Rayleigh scatterers, and their experimental cross-section spectra can be treated appoximately as $\sigma(\lambda) = a\lambda^{-4}$ where a is a constant (Figure S3, Supporting Information). However, neither RQDs nor SQDs are Rayleigh scatterers as assumed in earlier work (Figure S3, Supporting Information).[34] Third, the light scattering depolarization of the RQD is signficantly higher than both SQDs and fPSNPs. This phenomenon is consistent with the observations that the rod-shaped solvent molecules and gold NPs (AuNPs) invariably have higher light scattering depolarization than their respective spherical counterparts.[33,35]

Comparing and contrasting the RQD depolarization spectrum with that for rod-shaped molecule CS_2 and AuNPs is instructive. The scattering depolarization of CS_2 is totally wavelength-independent, and it is 0.5 crossing the entire UV−vis region,[35] while the scattering depolarization of gold nanorods is strongly wavelength-dependent,[33] so is that of RQD (Figure 2K). However, the peak scattering depolarizations of the rod-shaped AuNPs and QDs are vastly different. The peak scattering depolarization is 0.4 in a gold nanorod with an aspect ratio as small as 3.[33] In contrast, the peak scattering depolarization of the RQD is only 0.05 even when its aspect ratio is as large as 16.8 (Figure 1A). The fundamental mechanism governing the QD light scattering depolarization features is currently unclear. Nonetheless, the data obtained with the RQDs and SQDs provide further evidence that light scattering depolarization is sensitive to the scatterers' geometries.

Fluorophore Optical Properties in its Red Wavelength Region. Consistent with what has been observed in their blue wavelength regions, the UV−vis extinction spectra of moecular fluorophores R6G and EY in their red wavelength region can also be directly taken as their respective absorbance

DOI: 10.1021/acs.analchem.9b01803
Anal. Chem. 2019, 91, 8540−8548

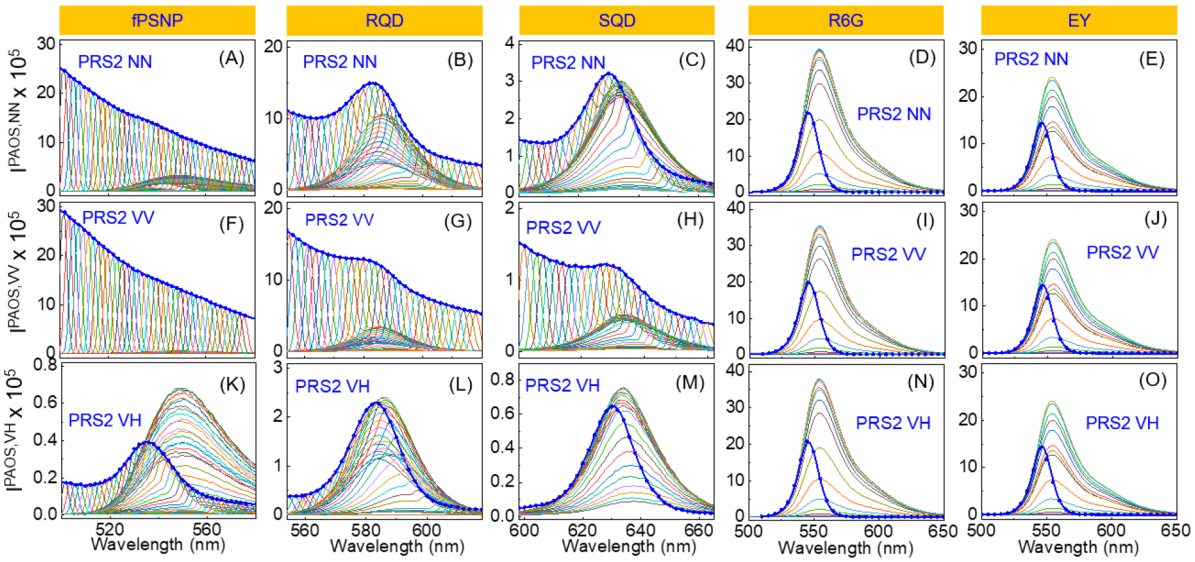

Figure 3. Comparisons of (1st row) as-acquired PAOS NN and PRS2 NN spectra, (2nd row) PAOS VV and PRS2 VV spectra, (3rd row) PAOS VH and PRS2 VH spectra for (1st column) RQD, (2nd column) SQD, (3rd column) R6G, and (4th column) EY in their red wavelength region. The solid blue line is the experimental PRS2 spectrum, and the blue dots are the PRS2 spectra reconstructed by taking the PAOS intensity at each excitation wavelength as the intensity of the reconstructed PRS2 spectrum at the resonance excitation and detection wavelength. Insert in F is the zoom-in spectrum that enables visualization of the fluorescence component.

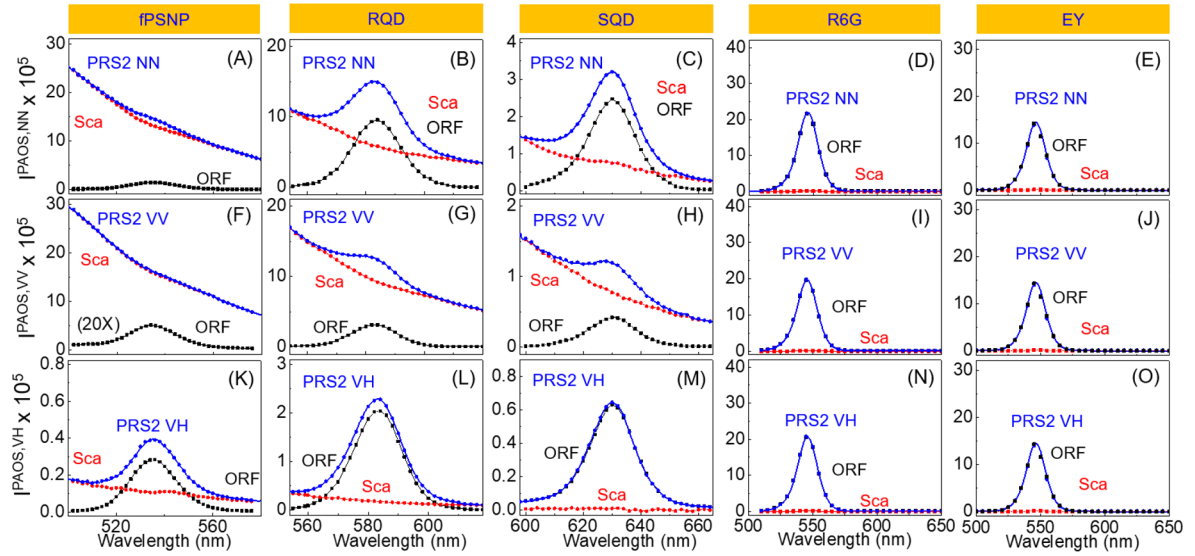

Figure 4. (Black) PRS2 fluorescence and (red) scattering component spectra derived from the experimental (blue) PAOS spectra for (1st column) RQD, (2nd column) SQD, (3rd column) R6G, and (4th column) Eosin Y. The data in the first, second, and third rows are derived from the PAOS spectra acquired with excitation and detection polarization of NN, VV, and VH, respectively.

spectrum since there are no detectable scattering features in the R6G and EY PAOS spectra obtained in their red-wavelength regions (Figure 1S,T). In contrast, PAOS spectra (Figure 1P–R) obtained with the NP fluorophores contain both fluorophore light scattering and fluorescence signals. This conclusion is further supported by the PAOS spectra obtained for all the model fluorophores in their red wavelength regions (Figure 3).

Comparing and contrasting the fluorophore PRS2 and PAOS spectra (Figure 3) is instructive. The experimental PRS2 spectra overlap nearly perfectly with that of the reconstructed PRS2 (Figure 3). The reconstructed PRS2 spectra (blue dots in the plots in Figure 3) were obtained by taking the PAOS spectral intensities at each excitation wavelength as the intensity of the reconstructed PRS2 spectrum. The excellent agreement between the experimental and reconstructed PRS2 spectra highlights the reproducibility of the PRS2 and PAOS measurements.

The PAOS-based PRS2 reconstruction method holds two key advantages over the direct experimental PRS2 acquisitions. First, the PAOS spectra used for the PRS2 reconstruction provide direct visual evidence that both light scattering and fluorescence can contribute to the fluorophore PRS2 spectra. In contrast, one can deduce the fluorescence and light scattering contribution to PRS2 signal through only indirect evidence either by the difference in the depolarization between fluorescence and light scattering[24] or by the difference in intensity dependence on the monochromator bandwidth

DOI: 10.1021/acs.analchem.9b01803
Anal. Chem. 2019, 91, 8540–8548

between the fluorescence and light scattering signal.[30] Second, the PAOS spectra enable one to directly separate the light scattering and fluorescence contribution to the experimental PRS2 spectrum and subsequently recontruct the fluorohore PRS2 light scattering and fluorescence component spectra (Figure 4). This light scattering peak is invariably centered at excitation wavelength and with a peak shape identical to the scattering peak observed in the PAOS spectra obtained with a pure scatterer such as the solvents and PSNP (Figure 1K−O). The decomposition of the fluorophore PAOS spectrum into its polarized fluorescence and light scattering component spectra (Figure 4) was performed by subtracting the scaled PSNP PAOS spectra from fluorophore PAOS spectrum (Figure S4, Supporting Information). The criterion for determining the scaling factor is that the resulting difference spectrum should contain no residual sharp peak on top of a broad fluorescence peak. Since there are no detectable light scattering features in the PAOS spectra obtained with R6G and EY (Figure 3), their experimental or reconstructed PRS2 spectra are their PRS2 fluorescence spectra. Third, the PAOS spectra offer direct evidence that when excited in the wavelength region the fluorophore both absorbs and emits; light scattering, ASSF, ORF, and SSF can all concurrently occur (Figure 1P−T and Figure 3).

The relative fluorescence and scattering contribution to the PRS2 spectra of the NP fluorophores depends strongly on the excitation and detection polarization (Figure 4). The scattering/fluorescence intensity ratio decreases from PRS2 VV, PRS2 NN, and then to PRS2 VH (Figure 4). This observation is consistent with the fact that fluorescence depolarization for fluorophores in solution is usally very high, close to unity for most small molecular fluorophores,[27] but the light scattering depolarization is commonly very small, as shown in Figure 2. The absence of a detectable scattering feature in the SQD PAOS VH is also consistent with spherical scatterers usually having negligible light scattering depolarization.[33,35]

Quantification of the light scattering cross-section using the fluorophore PRS2 light scattering spectra (red dots in Figure 4) is straightforward using the established PRS2 method,[27] for reasons that will be further illustrated later in this work. However, determination of the ORF cross-section on the basis of the fluorophore PRS2 fluorescence spectra requires modification of equations developed by assuming that the fluorescence signal in the PRS2 spectra is contributed by the fluorophore ORF alone,[27] or a combination of ORF and SSF without consideration of ASSF.[30] Mathematically, the fluorophore fluorescence PRS2 VV and VH spectra can be described using eq 1 and eq 2, respectively, while the fluorophore light scattering PRS2 VV and VH intensities are modeled with eqs 3 and 4, respectively.

$$I_{f,VV}^{PRS2,F}(\lambda, W) = I_o(\lambda, W)K(\lambda, W)B_V(\lambda, W)C_f \int_{\lambda-W/2}^{\lambda+W/2}\int_{\lambda-W/2}^{\lambda+W/2}\sigma_{f,VV}^{F}(\lambda_x, \lambda_m)\,d\lambda_m\,d\lambda_x \quad (1)$$

$$I_{f,VH}^{PRS2,F}(\lambda, W) = I_o(\lambda, W)K(\lambda, W)B_H(\lambda, W)C_f \int_{\lambda-W/2}^{\lambda+W/2}\int_{\lambda-W/2}^{\lambda+W/2}\sigma_{f,VH}^{F}(\lambda_x, \lambda_m)\,d\lambda_m\,d\lambda_x \quad (2)$$

$$I_{f,VV}^{PRS2,sca}(\lambda, W) = I_o(\lambda, W)K(\lambda, W)B_V(\lambda, W)C_f \int_{\lambda-W/2}^{\lambda+W/2}\sigma_{f,VV}^{Sca}(\lambda_x)\,d\lambda_x \quad (3)$$

$$I_{f,VH}^{PRS2,sca}(\lambda, W) = I_o(\lambda, W)K(\lambda, W)B_H(\lambda, W)C_f \int_{\lambda-W/2}^{\lambda+W/2}\sigma_{f,VH}^{Sca}(\lambda_x)\,d\lambda_x \quad (4)$$

Equations 1−4 are derived similarly to eqs 1 and 2 in a recent ratiometric bandwidth-varied PRS2 work.[30] C_f is the fluorophore concentration. The variables $I_{f,VV}^{PRS2}(\lambda,W)$, $I_{f,VH}^{PRS2}(\lambda,W)$, $I_o(\lambda,W)$, $K(\lambda,W)$, $B_V(\lambda,W)$, and $B_H(\lambda,W)$ are all defined identically as before.[30] The inclusion of parameter W in these variables is to reflect the fact that the values of these variables can depend on the monochromator wavelength bandwidth used in the resonance photon excitation and detection.[30]

$\sigma_{f,VV}^{F}(\lambda_x,\lambda_m)$ and $\sigma_{f,VH}^{F}(\lambda_x,\lambda_m)$ refer to the fluorophore fluorescence cross sections at the exact excitation wavelength of λ_x and exact detection wavelength of λ_m under excitation and detection polarization combinations of "VV" and "VH," respectively. The inclusion of two wavelength variables λ_x and λ_m in the fluorescence cross-section terms $\sigma_{f,VV}^{F}(\lambda_x,\lambda_m)$ and $\sigma_{f,VH}^{F}(\lambda_x,\lambda_m)$ indicates that the wavelength of the emitted photons can be different from the incident photons even at the resonance excitation and detection conditions. These two wavelength terms are needed because both PRS2 and PAOS spectra are conducted with a small but finite (not infinitely small) wavelength bandwidth. When excited in the wavelength region where the fluorophore both absorbs and emits, ASSF, ORF, and SSF occur when $\lambda_x > \lambda_m$, $\lambda_x = \lambda_m$, and $\lambda_x < \lambda_m$, respectively.

Equations 3 and 4, for parametrizing fluorophore scattering PRS2 VV and PRS2 VH signals, are identical to the light scattering terms in the earlier work,[27] but the fluorescence terms (eq 1 and eq 2) differ significantly from that the earlier ones.[27,30] In the recent BV-PRS2 method, the integration range of the inner integral varies from λ_x to $\lambda + W/2$. In this case, only the fluorophore ORF and SSF are considered.[30] By expanding the inner integration range from $\lambda - W/2$ to $\lambda + W/2$, the revised PRS2 method demonstrated herein takes full consideration of the ASSF, ORF, and SSF contribution to the fluorescence signal detected under the resonance conditions. The terms $\int_{\lambda-W/2}^{\lambda+W/2}\int_{\lambda-W/2}^{\lambda+W/2}\sigma_{f,VV}^{F}(\lambda_x, \lambda_m)\,d\lambda_m\,d\lambda_x$ and $\int_{\lambda-W/2}^{\lambda+W/2}\int_{\lambda-W/2}^{\lambda+W/2}\sigma_{f,VH}^{F}(\lambda_x, \lambda_m)\,d\lambda_m\,d\lambda_x$ in eqs 1 and 2 describe the integrated fluorescence cross-sections when the excitation and detection wavelengths both center at the same wavelength of λ and with an identical bandwidth of W. The inner integrals $\int_{\lambda-W/2}^{\lambda+W/2}\sigma_{f,VV}^{F}(\lambda_x, \lambda_m)\,d\lambda_m$ and $\int_{\lambda-W/2}^{\lambda+W/2}\sigma_{f,VH}^{F}(\lambda_x, \lambda_m)\,d\lambda_m$ refer to the emitted fluorescence cross sections being integrated from the excitation wavelength of $\lambda - W/2$ to $\lambda + W/2$ for each exact excitation wavelength λ_x. The outer integrals in $\int_{\lambda-W/2}^{\lambda+W/2}\int_{\lambda-W/2}^{\lambda+W/2}\sigma_{f,VV}^{F}(\lambda_x, \lambda_m)\,d\lambda_m\,d\lambda_x$ and $\int_{\lambda-W/2}^{\lambda+W/2}\int_{\lambda-W/2}^{\lambda+W/2}\sigma_{f,VH}^{F}(\lambda_x, \lambda_m)\,d\lambda_m\,d\lambda_x$ reflect the fact that the excitation wavelength varies from $\lambda - W/2$ to $\lambda + W/2$.

Since the detection wavelength bandwidth W in practical PAOS and PRS2 measurements is very small in comparison to

DOI: 10.1021/acs.analchem.9b01803
Anal. Chem. 2019, 91, 8540−8548

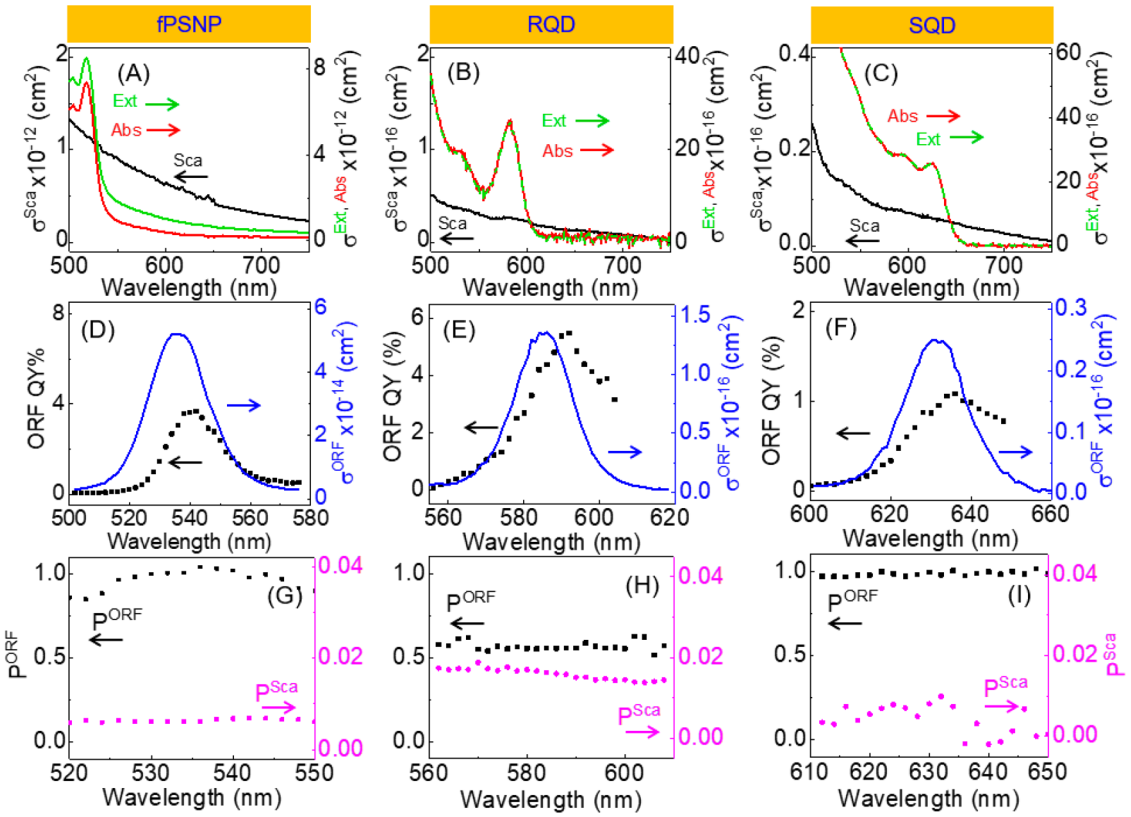

Figure 5. Optical constants of (1st column) fPSNP, (2nd column) RQD, and (3rd column) SQD in their respective red wavelength region. (1st row) UV−vis (green) extinction, (red) absorption, and (black) scattering cross-sections. (2nd row) ORF emission (blue) cross-sections and (black) ORF quantum yield (QY) spectrum. (3rd row) (red) scattering and (black) ORF depolarization. The spectra, axis, and name for each optical parameter are encoded with the same color.

the bandwidth of typical absorption, light scattering, and fluorescence peaks, one can approximate the material fluorescence and light scattering cross-sections $\sigma^{F}_{f,VV}(\lambda_x,\lambda_m)$, $\sigma^{F}_{f,VH}(\lambda_x,\lambda_m)$, $\sigma^{Sca}_{f,VV}(\lambda_x)$, and $\sigma^{Sca}_{f,VH}(\lambda_x)$ in the wavelength region from $\lambda - W/2$ to $\lambda + W/2$ as constants of $\sigma^{F}_{f,VV}(\lambda,\lambda)$, $\sigma^{F}_{f,VH}(\lambda,\lambda)$, $\sigma^{Sca}_{f,VV}(\lambda)$, and $\sigma^{Sca}_{f,VH}(\lambda)$, respectively. $\sigma^{F}_{f,VV}(\lambda,\lambda)$ and $\sigma^{F}_{f,VH}(\lambda,\lambda)$ are the fluorescence cross-sections at a resonance excitation and detection wavelength of λ; they can thus be simplified as $\sigma^{ORF}_{f,VV}(\lambda)$ and $\sigma^{ORF}_{f,VH}(\lambda)$, respectively. Under this condition, eqs 1−4 are converted into eqs 5−8 with simple mathematical manipulations (Supporting Information).

$$I^{PRS2,F}_{f,VV}(\lambda, W) = I_o(\lambda, W)K(\lambda, W)B_V(\lambda, W)C_f\sigma^{ORF}_{f,VV}(\lambda)W^2 \quad (5)$$

$$I^{PRS2,F}_{f,VH}(\lambda, W) = I_o(\lambda, W)K(\lambda, W)B_H(\lambda, W)C_f\sigma^{ORF}_{f,VH}(\lambda)W^2 \quad (6)$$

$$I^{PRS2,sca}_{f,VV}(\lambda, W) = I_o(\lambda, W)K(\lambda, W)B_V(\lambda, W)C_f\sigma^{Sca}_{f,VV}(\lambda)W \quad (7)$$

$$I^{PRS2,sca}_{f,VH}(\lambda, W) = I_o(\lambda, W)K(\lambda, W)B_H(\lambda, W)C_f \sigma^{Sca}_{f,VH}(\lambda)W \quad (8)$$

Dividing eq 6 by eq 5 and eq 8 by eq 7 with a rearrangement leads to eq 9 and eq 10 for quantification of the fluorophore ORF and light scattering depolarization spectrum,[27] respectively.

$$P^{ORF}_f(\lambda) = \frac{\sigma^{ORF}_{f,VH}(\lambda)}{\sigma^{ORF}_{f,VV}(\lambda)} = G(\lambda, W)\frac{I^{PRS2,F}_{f,VH}(\lambda, W)}{I^{PRS2,F}_{f,VV}(\lambda, W)} \quad (9)$$

$$P^{sca}_f(\lambda) = \frac{\sigma^{sca}_{f,VH}(\lambda)}{\sigma^{sca}_{f,VV}(\lambda)} = G(\lambda, W)\frac{I^{PRS2,sca}_{f,VH}(\lambda, W)}{I^{PRS2,sca}_{f,VV}(\lambda, W)} \quad (10)$$

where $G(\lambda,W) = B_V(\lambda,W)/B_H(\lambda,W)$ is the G-factor spectrum characterizing the instrument polarization bias, which can be readily quantified using a set of fluorescence samples emitting in different regions.[27] By using PSNP as the external reference, one can readily quantify the fluorophore light scattering and ORF cross-section using eqs 11 and 12, respectively. Detailed derivations of eqs 11 and 12 are shown in the Supporting Information.

$$\sigma^{sca}_f(\lambda) = \frac{(1 + 2P^{sca}_f(\lambda))}{(1 + 2P^{sca}_{PSNP}(\lambda))}\frac{C_{PSNP}I^{PRS2,sca}_{f,VV}(\lambda, W)}{C_fI^{PRS2,sca}_{PSNP,VV}(\lambda, W)}\sigma^{sca}_{PSNP}(\lambda) \quad (11)$$

$$\sigma^{ORF}_f(\lambda) = \frac{(1 + 2P^{ORF}_f(\lambda))}{(1 + 2P^{sca}_{PSNP}(\lambda))W}\frac{C_{PSNP}I^{PRS2,F}_{f,VV}(\lambda, W)}{C_fI^{PRS2,F}_{PSNP,VV}(\lambda, W)}\sigma^{sca}_{PSNP}(\lambda) \quad (12)$$

All the parameters on the right-hand side of eqs 11 and 12 are measurable. $\sigma^{sca}_{PSNP}(\lambda)$ is the PSNP scattering cross-section spectrum. Since PSNPs are pure light scatterers in the UV−vis region, $\sigma^{sca}_{PSNP}(\lambda)$ can be directly quantified using PSNP UV−vis extinction cross-section spectra measured with a UV−vis

DOI: 10.1021/acs.analchem.9b01803
Anal. Chem. 2019, 91, 8540−8548

spectrophotometer.[27] The $P_f^{ORF}(\lambda)$ and $P_f^{sca}(\lambda)$ are quantified using eqs 9 and 10, respectively. $I_{f,VV}^{PRS2,F}(\lambda,W)$ and $I_{f,VV}^{PRS2,sca}(\lambda,W)$ are the recontructed fluorophore PRS2 fluorescence and light scattering VV spectra, respectively. $I_{PSNP,VV}^{PRS2,sca}(\lambda,W)$ is the experimental PRS2 VV spectra obtained with PSNP.

The equation for computing the light scattering cross-section derived here (eq 11) is identical to that (eq 39) in the initial PRS2 publication.[27] However, there is a small but critical difference in the equation for computing the fluorophore ORF cross-section. The monochromator bandwidth term W shown in the denominator of eq 12 in this work is missing in eq 40 in the initial PRS2 work where neither the SSF nor ASSF contribution to the fluorophore PRS2 fluorescence signal was considered.[27]

Using eqs 11 and 12 and the fluorophore PRS2 fluorescence spectra $I_{f,VV}^{PRS2,F}(\lambda,W)$ and fluorophore PRS2 scattering spectra $I_{f,VV}^{PRS2,sca}(\lambda,W)$ shown in Figure 4, the light scattering and ORF cross-section spectra were quantified for the three NP fluorophores (Figure 5) and two molecular fluorophores in their red-wavelength regions (Figure S5, Supporting Information). The fluorophore absorption cross-section spectrum is quantified by subtracting the fluorophore light scattering cross-section spectrum from its extinction cross-section spectrum (Figure 5A−C and Figure S5A,B). The fluorophore ORF quantum yield spectrum (QY) is determined using the equation ORF $QY(\lambda) = \sigma^{ORF}(\lambda)/\sigma^{abs}(\lambda)$, the ratio between the fluorophore ORF fluorescence cross-section spectrum versus absorption cross-section spectrum in the wavelength region that the fluorophore both absorbs and emits. Since the signals of R6G and EY PRS2 spectra are completely dominated by the fluoroescence feature, their IFE- and solvent-background-corrected PRS2 spectra were used directly for calculating the fluorophore ORF depolarization, cross-sections, and QY (Figure S5, Supporting Information). The fluorophore ORF and light scattering depolarization spectra (Figure 5I−K and Figure S5E,F) are computed using eqs 9 and 10, respectively.

Several observations from Figure 5 and Figure S5 (Supporting Information) are worth noting. fPSNP has drastically higher extinction, scattering, and absorption and ORF emission cross-sections than their respective counterparts for both the QDs and molecular fluorophores (Figure 5 and Figure S5, Supporting Information). The scattering cross-section of fPSNP at 500 nm excitation wavelength is more than 4 orders of magnitude higher than that for the RQD and SQD (Figure 5A−-C), which is due most likely to the fact that fPSNP is much larger than both RQDs and SQDs. The large fPSNP extinction, absorption, and ORF emission cross sections (Figure 5A−C) are due to the fact that each fPSNP contains multiple molecular fluorophores. According to the vendor, the fPSNP contains a mixture of fluorophores of a rhodamine and Alexa 532. The fact that fPSNP has a peak ORF cross-section (Figure 5E) ∼3000 times higher than that of both R6G and EY (Figure S5C,D, Supporting Information) indicates that the brightness of one fPSNP is comparable to ∼3000 molecular fluorophore molecules under the on-resonance excitation and detection conditions at their respective peak ORF wavelengths.

The average ORF depolarization of the RQDs in its ORF active region is 0.6 ± 0.06 (Figure 5H), which is signficantly smaller than that of other model fluoropores including the SQDs (Figure 5I). The ORF depolarizations for the other fluorophores are all close to unity crossing their entire ORF-active region. Fluorescence depolarization is related to the fluorophore mobility and fluorescence lifetime.[36−40] A detailed reason why RQDs have such a small ORF depolarization is currently unclear. However, this result suggests that the fluorescence depolarization can be an effective spectral marker for differentiating RQDs and SQDs. The fact that the RQDs have higher light scattering depolarization than both SQDs and fPSNPs (Figure 5 (I−K)) in their red wavelength region is consistent again with the fact that rod-shape scatterers have higher scattering depolarization than the spherical ones.

Up to date, we have presented three methods for differentiating and separating light scattering and fluorescence contributions to the sample PRS2 spectra. The first is the spectral subtraction method that works only under the assumption that the fluorophore PRS2 VH features are due entirely to its fluorescence.[27] This assumption is valid only for well-dispersed molecular fluorophores that have no detectable light scattering features in their PRS2 VH spectrum, but it is unreliable for the NP fluorophores used in this work. The second is the recent bandwidth varied-PRS2 (BV-PRS2) method.[30] While the BV-PRS2 technique is a self-sufficient method enabling one to compute light scattering and ORF cross-sections and depolarization regardless of the fluorophore fluorescence and light scattering depolarization, it provides no insights to the origins of the fluorescence detected in the PRS2. The third, which is the current PAOS-based approach, is also a self-sufficient method. The key advantage of this PAOS-based method is that it enables direct visualization and separation of the light scattering and fluorescence contribution to fluorophore PRS2 spectra. This visualization has been critical for revealing the fact that the fluorescence in the PRS2 spectra comprises ASSF, ORF, and SSF contributions, not just ORF in the initial PRS2 technique,[27] or only ORF and SSF assumed in the BV-PRS2 technique.[30]

■ CONCLUSIONS

In summary, we demonstrated a divide-and-conquer strategy in combination with a PAOS spectral acquisition method for experimental quantification of the fluorophore optical constant spectra including their extinction, absorption, scattering, and ORF cross-section spectra; scattering and fluorescence depolarization spectra; and ORF QY spectra. This strategy combines efficiency and accuracy. In their blue wavelength regions, fluorophores are simultaneously photon absorbers and scatterers, but not emitters. Therefore, one can directly use the experimental PRS2 spectrum to decompose the fluorophore UV−vis extinction spectrum into its absorption and scattering component spectra. In contrast, in their red wavelength region, the fluorophores are simultaneous photon absorbers, scatterers, and fluorescence emitters. In this case, the somewhat more time-consuming PAOS spectral acquisition is needed to reconstruct the fluorophore PRS2 fluorescence and light scattering spectra for determination of the fluorophore optical properties. Since the PAOS spectral acquisition is performed only in the fluorophore red-wavelength region, a complete set of PAOS NN, VV, or VH spectra can be taken within 20 min of spectral acquisition time. Besides offering critical new insight that fluophore ASSF, ORF, SSF, and light scattering can all contribute to signal detected under resonance excitation and detection conditions, the methodology provided in this work should be of broad signficance to the quantification of the optical properties of various fluorophores in solutions.

DOI: 10.1021/acs.analchem.9b01803
Anal. Chem. 2019, 91, 8540−8548

■ ASSOCIATED CONTENT

Supporting Information

The Supporting Information is available free of charge on the ACS Publications website at DOI: 10.1021/acs.analchem.9b01803.

Synthesis and characterization of QDs; UV−vis extinction and absorption cross-section spectra of R6G and EY; comparison of experimental scattering cross-section spectra of fPSNP, SQD, and RQD and modeled Rayleigh scattering spectra; example decomposition of experimental PAOS spectrum into its fluorescence and scattering component spectrum; conversion of eqs 1−4 into eqs 5−8; derivation of eq 11 and eq 12; experimental optical constant spectra for R6G and EY (PDF)

■ AUTHOR INFORMATION

Corresponding Author

*Tel: (662) 325-6752. E-mail: Dongmao@chemistry.msstate.edu, dmzhang@mail.xhu.edu.cn.

ORCID

Shengli Zou: 0000-0003-1302-133X

Ou Chen: 0000-0003-0551-090X

Dongmao Zhang: 0000-0002-2303-7338

Notes

The authors declare no competing financial interest.

■ ACKNOWLEDGMENTS

This work was supported by NSF funds (CHE 1151057 and EPS-0903787) provided to D.Z. and ACS Division of Analytical Chemistry Summer Graduate Fellowship sponsored by the Society for Analytical Chemists of Pittsburgh provided to J.X.X. S.Z. thanks the Extreme Science and Engineering Discovery Environment (XSEDE) Open Science Grid (OSG) as the service provider. O.C. acknowledges the Brown University startup fund and IMNI seed fund.

■ REFERENCES

(1) Lan, G.; Ni, K.; Xu, Z.; Veroneau, S. S.; Song, Y.; Lin, W. *J. Am. Chem. Soc.* **2018**, *140*, 5670.

(2) Song, B.; Wang, H.; Zhong, Y.; Chu, B.; Su, Y.; He, Y. *Nanoscale* **2018**, *10*, 1617.

(3) Ren, X.; Liang, W.; Wang, P.; Bunker, C. E.; Coleman, M.; Teisl, L. R.; Cao, L.; Sun, Y.-P. *Carbon* **2019**, *141*, 553.

(4) Crisp, R. W.; Kirkwood, N.; Grimaldi, G.; Kinge, S.; Siebbeles, L. D. A.; Houtepen, A. J. *ACS Appl. Energy Mater.* **2018**, *1*, 6569.

(5) Yuan, Y.; Zhu, H.; Wang, X.; Cui, D.; Gao, Z.; Su, D.; Zhao, J.; Chen, O. *Chem. Mater.* **2019**, *31*, 2635.

(6) Sreejith, S.; Kishor, R.; Abbas, A.; Thomas, R.; Yeo, T.; Ranjan, V. D.; Vaidyanathan, R.; Seah, Y. P.; Xing, B.; Wang, Z.; Zeng, L.; Zheng, Y.; Lim, C. T. *ACS Appl. Mater. Interfaces* **2019**, *11*, 4867.

(7) Nagaoka, Y.; Tan, R.; Li, R.; Zhu, H.; Eggert, D.; Wu, Y. A.; Liu, Y.; Wang, Z.; Chen, O. *Nature* **2018**, *561*, 378.

(8) Nagaoka, Y.; Zhu, H.; Eggert, D.; Chen, O. *Science* **2018**, *362*, 1396.

(9) Zhou, Z.; Liu, X.; Yue, L.; Willner, I. *ACS Nano* **2018**, *12*, 10725.

(10) Origuchi, S.; Kishimoto, M.; Yoshizawa, M.; Yoshimoto, S. *Angew. Chem., Int. Ed.* **2018**, *57*, 15481.

(11) Chai, J.; Yang, S.; Lv, Y.; Chen, T.; Wang, S.; Yu, H.; Zhu, M. *J. Am. Chem. Soc.* **2018**, *140*, 15582.

(12) Bhattacharyya, B.; Pandey, A. *J. Am. Chem. Soc.* **2016**, *138*, 10207.

(13) Böhm, M. L.; Jellicoe, T. C.; Tabachnyk, M.; Davis, N. J. L. K.; Wisnivesky-Rocca-Rivarola, F.; Ducati, C.; Ehrler, B.; Bakulin, A. A.; Greenham, N. C. *Nano Lett.* **2015**, *15*, 7987.

(14) Kim, S.; Marshall, A. R.; Kroupa, D. M.; Miller, E. M.; Luther, J. M.; Jeong, S.; Beard, M. C. *ACS Nano* **2015**, *9*, 8157.

(15) Geissler, D.; Wuerth, C.; Wolter, C.; Weller, H.; Resch-Genger, U. *Phys. Chem. Chem. Phys.* **2017**, *19*, 12509.

(16) van de Hulst, H. C. *Light Scattering by Small Particles*; Dover Publications, 2012.

(17) Andrews, D. L.; Dávila Romero, L. C.; Stedman, G. E. *Phys. Rev. A: At., Mol., Opt. Phys.* **2003**, *67*, No. 055801.

(18) Johnson, R. C.; Li, J.; Hupp, J. T.; Schatz, G. C. *Chem. Phys. Lett.* **2002**, *356*, 534.

(19) Gangemi, C. M. A.; D'Agostino, B.; Randazzo, R.; Gaeta, M.; Fragalà, M. E.; Purrello, R.; D'Urso, A. *J. Porphyrins Phthalocyanines* **2018**, *22*, 581.

(20) Yue, Q.; Tao, L.; Hou, Y.; Zhang, C.; Wang, Y.; Hong, M.; Li, C.-Z. *Nanomedicine* **2018**, *13*, 2301.

(21) Chu, J.-Q.; Zhang, L.-M.; Zhu, L.-N.; Kong, D.-M.; Cui, Y.-X. *Nucleic Acids Res.* **2019**, *47*, 2727.

(22) Pasternack, R.; Collings, P. *Science* **1995**, *269*, 935.

(23) Arteaga, O.; Canillas, A.; El-Hachemi, Z.; Crusats, J.; Ribó, J. M. *Nanoscale* **2015**, *7*, 20435.

(24) Athukorale, S. A.; Zhou, Y.; Zou, S.; Zhang, D. *Anal. Chem.* **2017**, *89*, 12705.

(25) Xu, J. X.; Vithanage, B. C. N.; Athukorale, S. A.; Zhang, D. *Analyst* **2018**, *143*, 3382.

(26) Nettles, C. B.; Hu, J.; Zhang, D. *Anal. Chem.* **2015**, *87*, 4917.

(27) Siriwardana, K.; Vithanage, B. C. N.; Zou, S.; Zhang, D. *Anal. Chem.* **2017**, *89*, 6686.

(28) Williams, P. F.; Rousseau, D. L.; Dworetsky, S. H. *Phys. Rev. Lett.* **1974**, *32*, 196.

(29) Wu, F. Y.; Grove, R. E.; Ezekiel, S. *Phys. Rev. Lett.* **1975**, *35*, 1426.

(30) Xu, J. X.; Hu, J.; Zhang, D. *Anal. Chem.* **2018**, *90*, 7406.

(31) Chen, O.; Zhao, J.; Chauhan, V. P.; Cui, J.; Wong, C.; Harris, D. K.; Wei, H.; Han, H. S.; Fukumura, D.; Jain, R. K.; Bawendi, M. G. *Nat. Mater.* **2013**, *12*, 445.

(32) Carbone, L.; Nobile, C.; De Giorgi, M.; Sala, F. D.; Morello, G.; Pompa, P.; Hytch, M.; Snoeck, E.; Fiore, A.; Franchini, I. R.; Nadasan, M.; Silvestre, A. F.; Chiodo, L.; Kudera, S.; Cingolani, R.; Krahne, R.; Manna, L. *Nano Lett.* **2007**, *7*, 2942.

(33) Xu, J. X.; Siriwardana, K.; Zhou, Y.; Zou, S.; Zhang, D. *Anal. Chem.* **2018**, *90*, 785.

(34) Geissler, D.; Wurth, C.; Wolter, C.; Weller, H.; Resch-Genger, U. *Phys. Chem. Chem. Phys.* **2017**, *19*, 12509.

(35) Athukorale, S. A.; Zhou, Y.; Zou, S.; Zhang, D. *Anal. Chem.* **2017**, *89*, 12705.

(36) Jameson, D. M.; Ross, J. A. *Chem. Rev.* **2010**, *110*, 2685.

(37) Tice, D. B.; Weinberg, D. J.; Mathew, N.; Chang, R. P. H.; Weiss, E. A. *J. Phys. Chem. C* **2013**, *117*, 13289.

(38) Hadar, I.; Philbin, J. P.; Panfil, Y. E.; Neyshtadt, S.; Lieberman, I.; Eshet, H.; Lazar, S.; Rabani, E.; Banin, U. *Nano Lett.* **2017**, *17*, 2524.

(39) Zhang, Y.; Miao, L.; Wang, H.-F. *Anal. Chem.* **2016**, *88*, 9714.

(40) Gawełczyk, M.; Syperek, M.; Maryński, A.; Mrowiński, P.; Dusanowski, Ł; Gawarecki, K.; Misiewicz, J.; Somers, A.; Reithmaier, J. P.; Höfling, S.; Sęk, G. *Phys. Rev. B: Condens. Matter Mater. Phys.* **2017**, *96*, 245425.

DOI: 10.1021/acs.analchem.9b01803
Anal. Chem. 2019, 91, 8540−8548